

THE HYDRODYNAMICS OF GAMMA-RAY BURST REMNANTS

ENRICO RAMIREZ-RUIZ^{1,2} AND ANDREW I. MACFADYEN^{1,3}

Draft version August 18, 2021

ABSTRACT

This paper reports on the results of a numerical investigation designed to address how the initially anisotropic appearance of a GRB remnant is modified by the character of the circumburst medium and by the possible presence of an accompanying supernova (SN). Axisymmetric hydrodynamical calculations of light, impulsive jets propagating in both uniform and inhomogeneous external media are presented, which show that the resulting dynamics of their remnants since the onset of the non-relativistic phase is different from the standard self-similar solutions. Because massive star progenitors are expected to have their close-in surroundings modified by the progenitor winds, we consider both free winds and shocked winds as possible external media for GRB remnant evolution. Abundant confirmation is provided here of the important notion that the morphology and visibility of GRB remnants are determined largely by their circumstellar environments. For this reason, their detectability is highly biased in favor of those with massive star progenitors; although, in this class of models, the beamed component may be difficult to identify because the GRB ejecta is eventually swept up by the accompanying SN. The number density of asymmetric GRB remnants in the local Universe could be, however, far larger if they expand in a tenuous interstellar medium, as expected for some short GRB progenitor models. In these sources, the late size of the observable, asymmetric remnant could extend over a wide, possibly resolvable angle and may be easier to constrain directly.

Subject headings: gamma-rays: bursts – supernova remnants – hydrodynamics – shock waves – ISM: structure

1. INTRODUCTION

Relativistic jets are common in the astrophysical environment. Objects known or suspected to produce them include radio galaxies and quasars (Begelman et al. 1984), microquasars (Mirabel & Rodriguez 1999) and gamma-ray bursts (Gorosabel et al. 2006). An important difference between jets of quasars or microquasars is that active quasars often inject energy over extended periods of time into the jet while GRB sources are impulsive. Although quasar jets remain highly collimated throughout their lifetimes, GRB jets decelerate and expand significantly once they become nonrelativistic. Expansion into a uniform medium has been well studied (Ayal & Piran 2001), but the interaction of a GRB remnant with a nonuniform medium remains poorly understood.

Much of our effort in this paper is therefore dedicated to determining how the morphology and dynamics of young GRB remnants is modified by the character of the circumburst medium. Some of the questions at the forefront of attention include the effects of the external medium and the degree to which GRB remnant dynamics and structures are modified by the presence of an accompanying supernova. We address both of these issues here. Because massive stars are expected to have their close-in surroundings modified by the progenitor winds, we consider both free winds and shocked winds as possible surrounding media for the GRB remnant evolution. Detailed hydrodynamic simulations of this interaction are presented in §§4 and 6, while a brief description of the numerical methods and the initial models is given in §2. For completeness, the interaction with a constant-density medium is discussed in §3. The role of supernova explosions in shaping

the evolution and morphology of GRB remnants is discussed in §5. The effects of a nonspherical circumburst medium are briefly addressed in §4. Discussion and conclusions are presented in §7.

2. NUMERICAL METHODS AND INITIAL MODEL

2.1. *The Underlying Dynamics*

For simplicity, let's consider a uniform GRB jet with sharp edges and a half-opening angle θ_θ , with an initial value of θ_0 . The typical angular size, R_\perp , of the jet at $t < t_\theta$, where t_θ is the time at which the jet's Lorentz factor γ drops to θ_0^{-1} , is the same as for a spherical flow:

$$R_\perp(t) \propto \left(\frac{E_{\text{iso}}}{A}\right)^{\frac{1}{2(4-k)}} t^{\frac{5-k}{2(4-k)}} \propto \left(\frac{E}{A}\right)^{\frac{1}{2(3-k)}} t_j^{\frac{-1}{2(4-k)}} t^{\frac{5-k}{2(4-k)}} \quad (1)$$

for an external density profile $\rho_{\text{ext}} = Ar^{-k}$ (Granot, Ramirez-Ruiz & Loeb 2005). Here E is the *true* kinetic energy content of the jet, and $E_{\text{iso}} = f_b^{-1}E$ is the isotropic equivalent energy where $f_b \approx \theta_0^2/2$ is the beaming factor. At these early times, the flow is described by the Blandford-McKee (1976) self-similar solution, which provides an accurate expression for the temporal evolution of the observed image size:

$$R_\perp(t) = 4 \times 10^{16} \left(\frac{E_{\text{iso},52}}{n_0}\right)^{1/8} \left(\frac{t_{\text{days}}}{1+z}\right)^{5/8} \text{ cm} \quad (2)$$

for constant density medium ($k = 0$) with $n = 1 n_0 \text{ cm}^{-3}$ ($\rho = 1.67 \times 10^{-24} \rho_0 \text{ g cm}^{-3}$), and

$$R_\perp(t) = 2.5 \times 10^{16} \left(\frac{E_{\text{iso},52}}{A_*}\right)^{1/4} \left(\frac{t_{\text{days}}}{1+z}\right)^{3/4} \text{ cm} \quad (3)$$

for a stellar wind environment ($k = 2$) with $A_* = A/5 \times 10^{11} \text{ g cm}^{-1}$.

¹ Institute for Advanced Study, Einstein Drive, Princeton, NJ 08540, USA

² Department of Astronomy and Astrophysics, University of California, Santa Cruz, CA 95064, USA

³ CCPP, Department of Physics, New York University, 4 Washington Place, New York, NY 10003, USA

Notice that even in the most optimistic cases, the characteristic size of a GRB image is only of order 1μ as about a day after the GRB at the Hubble distance (Granot & Loeb 2001), and so it cannot be resolved by existing telescopes. Obviously, the challenge is made easier for nearby sources, where the late size of the observable remnant could extend over a wide, possibly resolvable angle (Oren et al. 2004; Granot & Ramirez-Ruiz 2004; Granot, Ramirez-Ruiz & Loeb 2005). At late times $t > t_{\text{NR}}$, where t_{NR} is the nonrelativistic transition time, the jet is expected to gradually approach the Sedov-Taylor self-similar solution, asymptotically reaching $R_{\perp}(t) \propto (E/A)^{1/(5-k)} t^{2/(5-k)}$. At $t_{\theta} < t < t_{\text{NR}}$ there is, however, a large uncertainty in the hydrodynamic evolution of the jet, and in particular in its rate of sideways expansion.

To illustrate the importance of sideways expansion on the evolution of the observed image, let's consider two extreme assumptions: (i) relativistic lateral expansion in the comoving frame (Rhoads 1999; Sari et al. 1999) for which $\theta_{\theta} \approx \max(\theta_0, \gamma^{-1})$ so that at $t_{\theta} < t < t_{\text{NR}}$ we have $\gamma \approx \theta_{\theta}^{-1} \approx \theta_0^{-1} \exp(-R/R_{\theta})$, and (ii) little or no lateral expansion, $\theta_{\theta} \approx \theta_0$ for $t < t_{\text{NR}}$, in which case appreciable lateral expansion occurs only when the jet becomes sub-relativistic and gradually approaches spherical symmetry.

For relativistic lateral expansion, $\theta_{\theta} \sim 1$ at $t_{\text{NR}} = t_{\text{NR}}(E)$, where $R_{\text{NR}}(E) = ct_{\text{NR}}(E) = [(3-k)E/4\pi Ac^2]^{1/(3-k)}$ and the jet radius will be similar to that of the Sedov-Taylor solution, $R_{\text{ST}}(E, t) \sim (Et^2/A)^{1/(5-k)}$. In this case, one expects the flow to approach spherical symmetry only after a few dynamical times. This is probably not the case as clearly illustrated by the results of numerical simulations (Granot et al. 2001; Cannizzo et al. 2004; Granot 2007) showing only modest lateral expansion as long as the jet is relativistic. If lateral expansion is neglected, the jet becomes sub-relativistic only at

$$R_{\text{NR}}(E_{\text{iso}}) = ct_{\text{NR}}(E_{\text{iso}}) = \left[\frac{(3-k)E_{\text{iso}}}{4\pi Ac^2} \right]^{1/(3-k)}. \quad (4)$$

For expansion in a constant density medium ($k=0$), eq. (4) can be rewritten as

$$R_{\text{NR}}(E_{\text{iso}}) = 0.3 \left(\frac{E_{51}}{\rho_0} \right)^{1/3} \left(\frac{f_b^{-1}}{30} \right)^{1/3} \text{ pc}, \quad (5)$$

while for a wind medium ($k=2$), it becomes

$$R_{\text{NR}}(E_{\text{iso}}) = 2 \left(\frac{E_{51}}{A_*} \right) \left(\frac{f_b^{-1}}{30} \right) \text{ pc}. \quad (6)$$

From eq. (4) it follows that $R_{\text{NR}}(E_{\text{iso}})$ is a factor of $\sim (E_{\text{iso}}/E)^{1/(3-k)} = f_b^{-1/(3-k)} \sim \theta_0^{-2/(3-k)}$ larger than $R_{\text{NR}}(E) = ct_{\text{NR}}(E)$ and a factor of $\sim f_b^{-1/(5-k)} \sim \theta_0^{-2/(5-k)}$ larger than $R_{\text{ST}}[E, t_{\text{NR}}(E_{\text{iso}})]$. Thus eq. (4) simply states that the jet keeps its original opening angle, $\theta_{\theta} \approx \theta_0$ until $t_{\text{NR}}(E_{\text{iso}})$, and hence at this time the jet is still far from being spherical. Thus, once the jet becomes sub-relativistic, we expect it to expand sideways significantly, and become roughly spherical only when it has increased its radius by a factor of ψ . This should occur roughly at a time t_{sph} when $R_{\text{ST}}(E, t_{\text{sph}}) = \psi R_{\text{NR}}(E_{\text{iso}})$:

$$\frac{t_{\text{sph}}}{t_{\text{NR}}} (E_{\text{iso}}) \approx f_b^{-1/2} \psi^{(5-k)/2} \approx \sqrt{2} \theta_0^{-1} \psi^{(5-k)/2}. \quad (7)$$

This is a factor of $\sim f_b^{-1/2} \approx 14(\theta_0/0.1)^{-1}$ larger than the expected transition time for relativistic lateral expansion in the

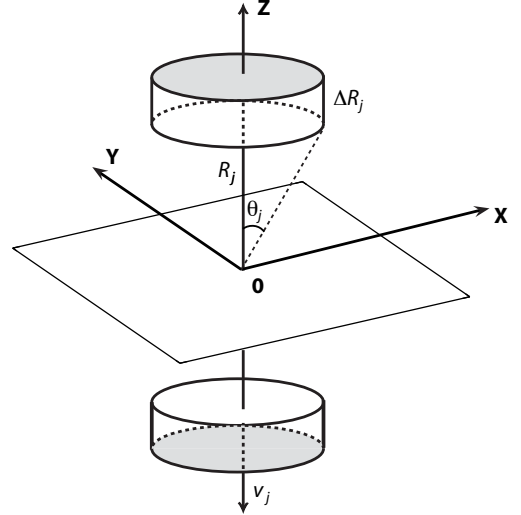


FIG. 1.— Schematic plot illustrating the numerical initiation of the GRB explosion.

comoving frame. In the sections that follows we present quantitative estimates of t_{sph} for GRB jets expanding in variety of circumburst environments.

2.2. Initial GRB Model

Common to all calculations is the initiation of the GRB explosion as two identical blobs expanding in opposite directions into the circumburst medium. Calculations were done in two dimensions in cylindrical geometry using the PPM adaptive mesh refinement code FLASH (ver 2.4). Both blobs and the circumburst medium are modeled by a cold, $\gamma = 5/3$, ideal gas. The initial configuration is as follows. The computational domain, as illustrated in Fig. 1, is an unprolonged cylinder in which the ejecta move along the symmetry axis. In the inner region of each of the pancakes, the ejecta mass, M_j is distributed uniformly. In all runs $v_j = 0.3c$, $\Delta R_j/R_j \approx 0.5$, $\theta_j \approx 0.5$, $M_j \approx 2E_j/v_j^2$ and $R_j \approx R_{\text{NR}}(E_{\text{iso}})$.

Without a detailed understanding of the exact shape and energy distribution of the ejecta, we have only an approximate description of how to construct the initial conditions. However, as clearly illustrated by Ayal & Piran (2001), the late time evolution of the ejecta is rather insensitive to uncertainties in the initial conditions. We have considered various initial densities, angular widths, and shapes of the collimated ejecta and found that these are indeed unimportant in determining the late morphology of the remnant. This stems from the fact that at late times the mass of the remnant is dominated by the circumburst gas, which washes out any variations in the initial conditions of the ejecta.

3. THE APPEARANCE OF A GRB REMNANT IN THE ISM

In this section we present a quantitative discussion of how the GRB remnant morphology is modified by expansion into a uniform medium. Expansion into a constant density medium is expected in a variety of progenitor models, in particular those related to short GRBs (Fryer et al. 1999; Bloom et al. 1999; Belczynski et al. 2006; Lee & Ramirez-Ruiz 2007). The discussion largely follows that of Ayal & Piran (2001), although analytical solutions are derived here to illustrate what may not be obvious from earlier derivations.

In the absence of characteristic scales in stellar ejecta and in

the ambient medium, self-similar, spherically symmetric solutions exist, and they are widely used to interpret observational data of GRB remnants (e.g. Waxman et al. 1998). However, as argued in §2.1, near the non-relativistic transition the remnant is far from being spherical and thus the Sedov-Taylor solution fails to provide an accurate description of the evolution of the GRB ejecta. A simple estimate for t_{sph} can be, however, obtain by assuming that the expansion of each of the collimated blobs is accurately described by a self-similar, spherically symmetric solution. Under these conditions, the problem reduces to depositing a finite amount of energy E at two different locations separated by a distance $R_j \sim R_{\text{NR}}(E_{\text{iso}})$. This is valid as long as the external medium is uniform around the explosion site. The evolution of the shock radius for each of the blobs will then follow:

$$R_{\text{ST}}(t) = \xi \left(\frac{E}{\rho_0} \right)^{1/5} t^{2/5} \quad (8)$$

with $\xi = 1.17$ for $\gamma = 5/3$. The ratio between the remnant width and height,

$$\varsigma = \frac{R_{\text{ST}}(t)}{R_{\text{ST}}(t) + R_j}, \quad (9)$$

will approach unity as the two blobs expand and merge. The GRB remnant will then become nearly spherical in shape after a time

$$t_{\text{sph}} \approx 243 \left(\frac{E_{51}}{\rho_0} \right)^{1/3} \left(\frac{f_b^{-1}}{30} \right)^{5/6} \left(\frac{\varsigma_{0.9}}{1 - \varsigma_{0.9}} \right)^{5/2} \text{ yr}, \quad (10)$$

when $\varsigma = 0.9\varsigma_{0.9}$. Obviously, the above calculation is only sketchy and should be taken as an order of magnitude figure, as it not only assumes that the mass of the collimated ejecta is negligible with respect to the swept-up gas but also neglects the presence of shocked material throughout the interaction region.

Detailed hydrodynamic simulations of the evolution of a GRB remnant in a uniform medium are presented in Fig. 2, where the density contours of the expanding collimated ejecta at various times in its hydrodynamical evolution are plotted. As the collimated ejecta collides with the ambient medium, a bow shock forms. The shock propagates in the direction of motion but also perpendicular to it and, over time, wraps around the expanding ejecta. Although initially the remnant may be highly nonspherical, the ratio between its width and height will approach unity as the two blobs expand, merge into a single structure and then finally become spherical in shape. The resultant structure will not be perfectly spherical as some density inhomogeneities around the equator resulting from the encounter remain visible. It will be, however, difficult to distinguish it (based on morphology alone) from a supernova remnant after about

$$t_{\text{sph}} \approx 3 \times 10^3 \left(\frac{E_{51}}{\rho_0} \right)^{1/3} \text{ yr}, \quad (11)$$

when $\varsigma \sim 0.9$. The governing parameters of the late evolution of the remnant are the initial energy of the jet, E , and the density of the ambient medium, ρ (Ayal & Piran 2001). As illustrated in Fig. 3, these two initial parameters can also determine the early evolution of the remnant for a fixed f_b .

4. EVOLUTION IN A CIRCUMSTELLAR WIND MEDIUM

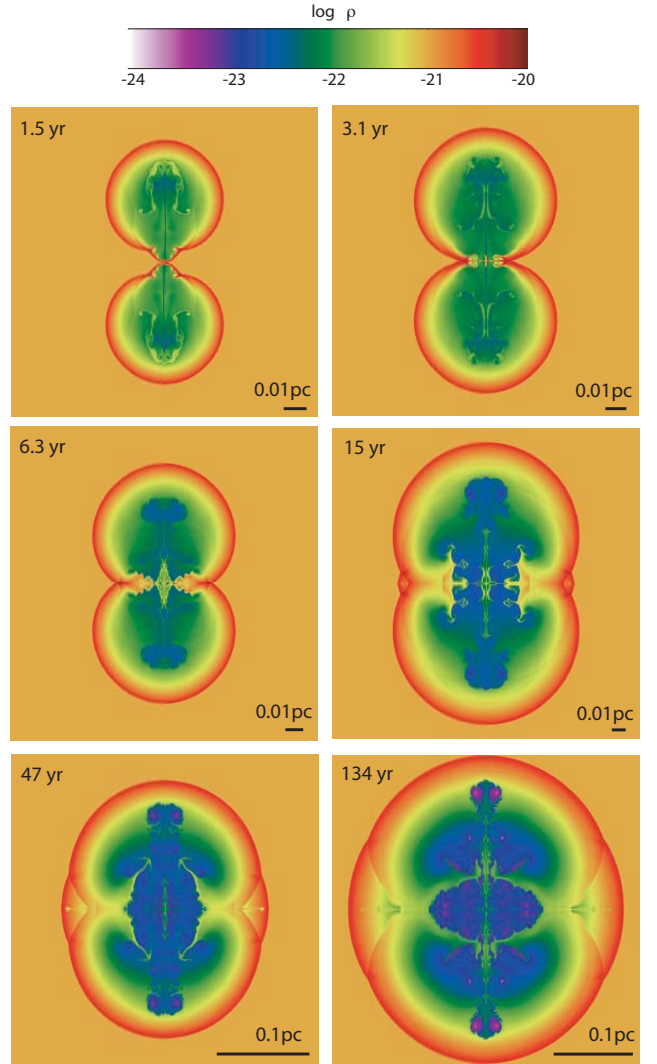


FIG. 2.— The evolution of a GRB remnant in a constant density medium. The ejecta, $E_j = 10^{50}$ erg, and surrounding ISM, $\rho_0 = 10^3$, are characterized by a $5/3$ adiabatic index. Shown are logarithmic density cuts in g cm^{-3} . Calculations were done in two-dimensional cylindrical coordinates for seven levels of refinement. The size of the computational domain was $(0.3 \text{ pc})^2$.

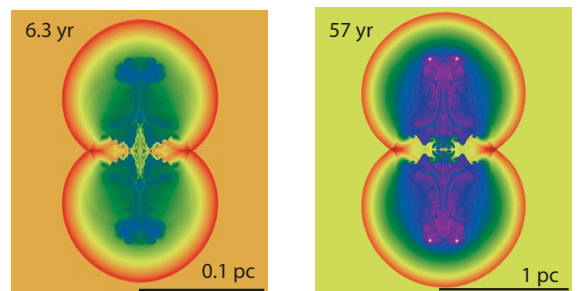


FIG. 3.— The evolution of a GRB remnant for $\rho_0 = 10^3$ (left) and $\rho_0 = 1$. Evolutionary ages in years are indicated in each frame together with corresponding size scales. As expected for a constant density medium, a unique combination of E , ρ and t has the dimensions of R .

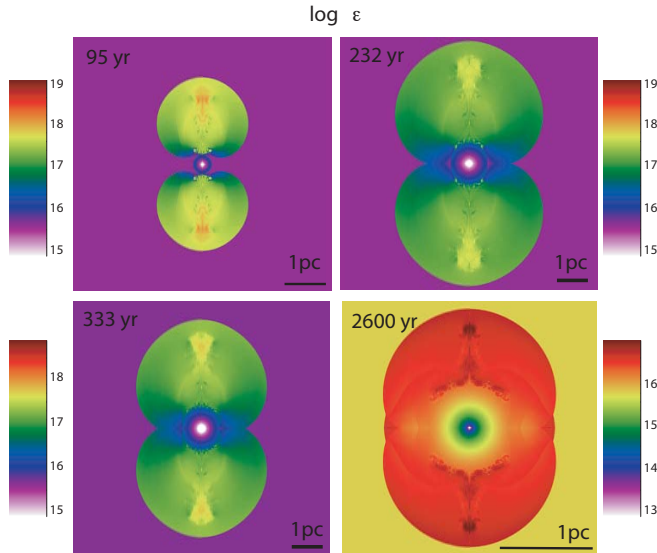


FIG. 4.— The evolution of a GRB remnant in a $1/r^2$ medium. The ejecta, $E_j = 10^{51}$ erg, and surrounding stellar wind medium ($v_w = 10^3$ km s $^{-1}$ and $\dot{M} = 2.5 \times 10^{-5} M_\odot$ yr $^{-1}$) are characterized by a $5/3$ adiabatic index. Shown is the evolution of the specific energy, ϵ , in erg/g. Calculations were done in two-dimensional cylindrical coordinates for ten levels of refinement. The size of the computational domain was $(16 \text{ pc})^2$.

If the progenitors of GRBs are massive stars then there is an analogy to the explosions of core collapse supernovae, for which there is abundant evidence that they interact with the winds from the progenitor stars. In most supernova cases, the radial range that is observed is only out to a few pc, such that the mass loss characteristics have not changed significantly during the time that mass is supplied to the wind (Chevalier & Li 2000). The density in the wind depends on the type of progenitor. Red supergiant stars, which are thought to be the progenitors of Type II supernovae, have slow dense winds. Wolf-Rayet stars, which are believed to be the progenitors of Type Ib/c supernovae and possibly of long GRBs (Woosley 1993; MacFadyen & Woosley 1999), have faster, lower-density winds. The winds from WRs are characterized by mass-loss rates $\dot{M} \approx 10^{-5} M_\odot$ yr $^{-1}$ and velocities $v_w \approx 10^3$ km s $^{-1}$ (Chiosi & Maeder 1986). In a steady, spherically symmetric wind, the stellar density is $\rho_{\text{ext}} = Ar^{-2}$, where $A = 5 \times 10^{11} (\dot{M}/10^{-5} M_\odot \text{ yr}^{-1}) (v_w/10^3 \text{ km s}^{-1})^{-1} \text{ g cm}^{-3}$. Note that for this choice of stellar wind parameters $A_* = 1$.

For this discussion we shall first assume the stellar wind is effectively spherical. The evolution of a GRB remnant in a stellar wind since the onset of the non-relativistic phase is summarized in Fig. 4. Similar resulting structures to those described in §3 are clearly seen. A bow shock forms as each blob collides with the stellar wind, which eventually wraps around the ejecta before the two expanding shells collide to form a single structure. However, because in a wind medium the swept-up mass increases only linearly with radius, the GRB remnant decelerates much more slowly than in a uniform medium. Moreover, in a wind medium, resistance to sideways expansion is increased. This is because the bow shock, as it wraps around the ejecta, encounters a steadily increasing ambient pressure. As a result, the remnant will

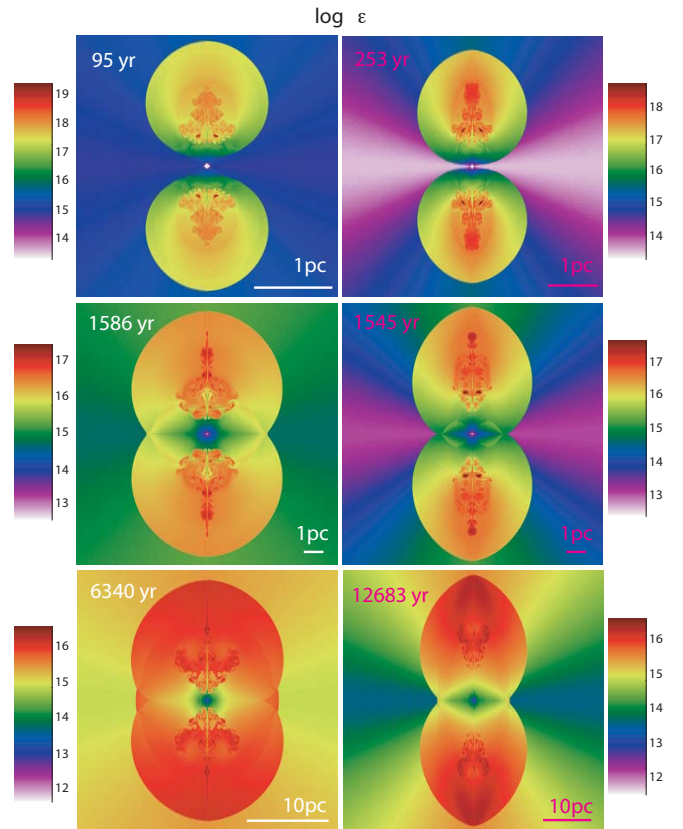


FIG. 5.— The evolution of a GRB remnant in a non-spherical $1/r^2$ medium. The ejecta, $E_j = 10^{51}$ erg, and surrounding stellar wind medium ($v_{\text{esc}} = 10^3$ km s $^{-1}$, $\zeta = 1$, $\varphi = 0.5$, $\dot{M} = 2.5 \times 10^{-5} M_\odot$ yr $^{-1}$, and $\Omega = 0.8$) are characterized by a $5/3$ adiabatic index. Shown is the evolution of the specific energy, ϵ , in erg/g. Calculations were done in two-dimensional cylindrical coordinates for seven levels of refinement. The size of the computational domain was $(30 \text{ pc})^2$.

become roughly spherical only after a time

$$t_{\text{sph}} \approx 5 \times 10^4 \left(\frac{E_{51}}{A_*} \right) \text{ yr}, \quad (12)$$

when $\zeta \sim 0.9$. Beyond this point, the evolution will evolve into a classical Sedov-Taylor supernova remnant evolution.

The estimate given by equation (12) could be inaccurate for a number of reasons. Depending upon the wind history of the progenitor star and the properties of the surrounding ISM, the density structure around $R_{\text{sph}} \approx 30 \text{ pc}$ could be quite complicated. The non-steady nature of the winds in massive stars together with the relatively large ISM pressure expected in star-forming regions, leaves open the possibility of interaction with denser material at much early times. In this case, the GRB remnant will start being decelerated by the external medium at a smaller radius than it would expanding into a free $1/r^2$ wind. Much of our effort in §6 will therefore be dedicated to determining the contribution of the presupernova ejecta of Wolf-Rayet stars to the circumburst environment, and describing how this external matter can affect the observable characteristics of GRB remnants.

Large-scale density gradients in the ambient medium could result in asymmetric, nonradial distortions. In this case, t_{sph} could be larger than that given by equation (12). For example, Fig. 5 shows the evolution of a GRB remnant in an asymmet-

ric wind, under the assumption that the progenitor star experiences non-spherical mass loss close to critical rotation: in other words, a scenario in which a slower and denser wind is confined to the equatorial plane. To compute the latitudinal dependence of the wind properties of a star close to critical rotation ideally requires multi-dimensional models of the star and its outflowing atmosphere, which are not available. Langer (1998), however, argued that the stellar flux and the radius might still vary only weakly from pole to the equator in very luminous stars. We therefore applied equations similar to those found by Bjorkman & Cassinelli (1993) for winds of rotating stars in the limit of large distance from the star:

$$v_{\infty}(\theta) = \zeta v_{\text{esc}} (1 - \Omega \sin\theta)^{\varphi}, \quad (13)$$

where we set the parameters defined in Bjorkman & Cassinelli (1993) to $\zeta = 1$, $\varphi = 0.5$, $\Omega = v_{\text{rot}}/v_{\text{crit}} = 0.8$, and $v_{\text{crit}} = v_{\text{esc}}/\sqrt{2} = [GM_*(1 - \kappa)/R_*]^{1/2}$, with M_* and R_* being mass and radius of the star, and κ standing for the ratio L/L_{Edd} of stellar to Eddington luminosity. Under the above conditions, the GRB remnant expands more quickly and easily into the lower density wind at the poles, producing an increasingly asymmetric double-lobed structure.

Finally, the estimate given by equation (12) would be modified if the beamed GRB is accompanied by an underlying supernova, as expected in the collapsar model (MacFadyen & Woosley 1999; MacFadyen et al. 2001; Woosley & Bloom 2006). The large-angle SN outflow, responsible for exploding the star and producing the ^{56}Ni , would generally carry more energy and inertia than the relativistic jet itself (e.g., Soberg et al. 2004; Mazzali et al. 2006; Kaneko et al. 2007), so that the latter always overtakes it, and sweeps up the GRB ejecta. It is to this problem that we now turn our attention.

5. INTERACTION WITH AN UNDERLYING SUPERNOVAE

It seems likely that GRBs originate in a very small fraction of massive stars that undergo a catastrophic energy release event toward the end of their evolution. Expressly, the association of some GRBs with type Ic supernovae (e.g., Hjorth et al. 2003; Stanek et al. 2003; Pian et al. 2006) has pointed a finger at deaths of massive Wolf-Rayet stars as the cause of GRBs, or at least a subset thereof. The central engine is believed to give rise to a polar outflow with two components (MacFadyen & Woosley 1999; Ramirez-Ruiz et al. 2002; Woosley & Bloom 2006). One large-angle outflow (the SN), containing most of the energy and mass, is responsible for exploding the star and producing the ^{56}Ni to make the SN bright. A second outflow component (the GRB jet) occupies a narrower solid angle and probably contains less energy (which can range from comparable to much less), and most of its energy is in material with relativistic velocities (where the typical Lorentz factor of the material that carries most of the energy in this component can vary significantly among SN-GRBs).

The large-angle SN outflow, carrying more energy and inertia than the relativistic jet itself, will generally sweep up the GRB ejecta before it has been much decelerated. An order of magnitude estimate for t_{sph} can be obtain by assuming that the dynamics of the laterally-expanding, GRB ejecta is accurately described by a self-similar, spherically solution in a $1/r^2$ medium and that the SN outflow does not appreciably slow down. The evolution of the shock radius of the beamed

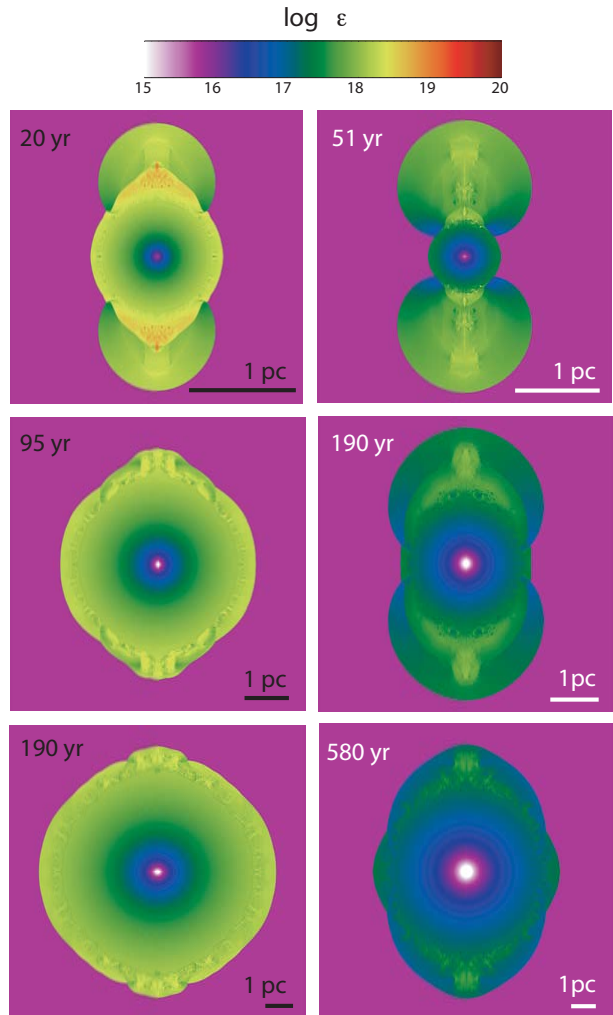


FIG. 6.— The evolution of a GRB remnant interacting with an underlying (slower expanding) spherical supernova. The stellar wind parameters as well as the GRB ejecta initial quantities are the same as in Fig. 4. Shown is the evolution of the specific energy, ϵ , in erg/g for two different SN explosion energies: 5×10^{51} erg (left) and 5×10^{50} erg (right). Calculations were done in two-dimensional cylindrical coordinates for ten levels of refinement. The size of the computational domain was $(30 \text{ pc})^2$.

remnant is then given by

$$R_{\text{ST}}(t) = \xi_w \left(\frac{E}{A} \right)^{1/3} t^{1/3} \quad (14)$$

with $\xi_w = 0.73$ for $\gamma = 5/3$. The GRB ejecta, as it clears the surrounding stellar matter, will be overtaking by the large scale-outflow SN at

$$t_{\text{sph}} \approx 910 \left(\frac{E_{51}}{A_*} \right) \left(\frac{\beta_{\text{SN}}}{0.1} \right)^{-3} \text{ yr}, \quad (15)$$

where $\beta = v_{\text{SN}}/c \ll 1$. After this time, the merged system will quickly become spherical. Yet it is clear that this simple estimate is inadequate as a model for the real complex dynamics, which necessitates the use of hydrodynamical calculations.

The evolution of a GRB remnant accompanied by an underlying supernova is shown in Fig. 6 for two different SN explosion energies. The stellar wind parameters are chosen so that they are equal to those displayed in Fig. 4. Com-

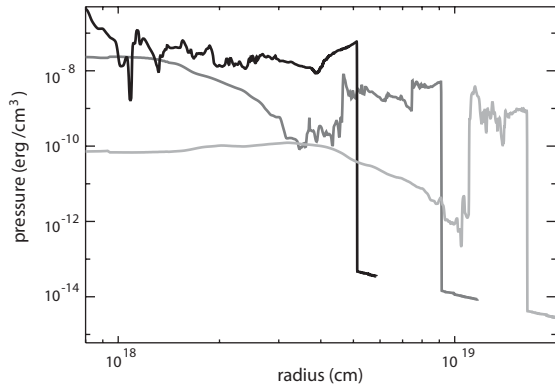


FIG. 7.— The pressure structure, along the z axis of a GRB remnant interacting with an underlying spherical supernova. The simulation is the same as in Fig. 6 for $E_{\text{SN}} = 5 \times 10^{50}$ erg and $t = 51, 190, 580$ yr.

pared to Fig. 4, significant structural differences appear when the SN outflow has grown significantly in size and it starts to overtake the laterally expanding GRB ejecta. Two illustrative cases are depicted: $E_{\text{SN}}: 5 \times 10^{51}$ erg (left panels) and 5×10^{50} erg (right panels). In both cases, the SN outflow carries more momentum than the beamed ejecta and drives a blast wave that eventually sweeps up all the GRB-shocked medium. This happens before the two beamed blobs collide on the equator. The merged system will become roughly spherical very soon after. For $E_{\text{SN}} = 5 \times 10^{51}$ erg (5×10^{50} erg), we obtain $t_{\text{sph}} \approx 250$ yr (3×10^3 yr). Not surprisingly, the presence of an underlying spherical supernova seriously modifies the simple estimate given by equation (12) and limits our ability to decipher the presence of a beamed component in a GRB explosion.

Prevailing to all these calculations is the initiation of the explosion as a pressure-driven blast wave by deposition of the explosion energy, E_{SN} , entirely as thermal energy. In the inner region, an ejecta mass, $M_{\text{SN}} \approx 5M_{\odot}$, are distributed uniformly. This may accurately model the Sedov-Taylor stage of SN remnant evolution after the ratio of swept-up mass to the mass of the original stellar ejecta exceeds roughly 19 (Fabian et al. 1983). In most cases, deceleration of the SN outflow will begin only sometime after the GRB ejecta has been swept up. As clearly seen in Fig. 7, the SN outflow at this early stage is not accurately described by the Sedov-Taylor solution. However, numerous tests show that our results are not strongly dependent upon the assumed mass of the SN ejecta or on whether kinetic energy rather than thermal energy is distributed (such that the velocity profile is linear; similar to the Sedov solution) in the inner region. None of these complications is likely to seriously modified our estimate for t_{sph} .

6. GRBs INSIDE PRE-EXISTING WIND-DRIVEN BUBBLES

So far we have considered either the uniform ambient medium case or the $1/r^2$ wind case on its own. However, since the winds in massive stars are non-steady, the density structure is more complex (Wijers 2001; Chevalier et al. 2004; Ramirez-Ruiz et al. 2005; van Marle et al. 2006). The preburst stellar wind depends on the evolutionary stages prior to (and during) the Wolf-Rayet stage (Ramirez-Ruiz et al. 2001). For Galactic stars, a standard evolutionary track is to start as an O star, evolve through a red supergiant (RSG) phase or luminous blue variable (LBV) phase with considerable mass loss, and ending as a Wolf-Rayet star (García-

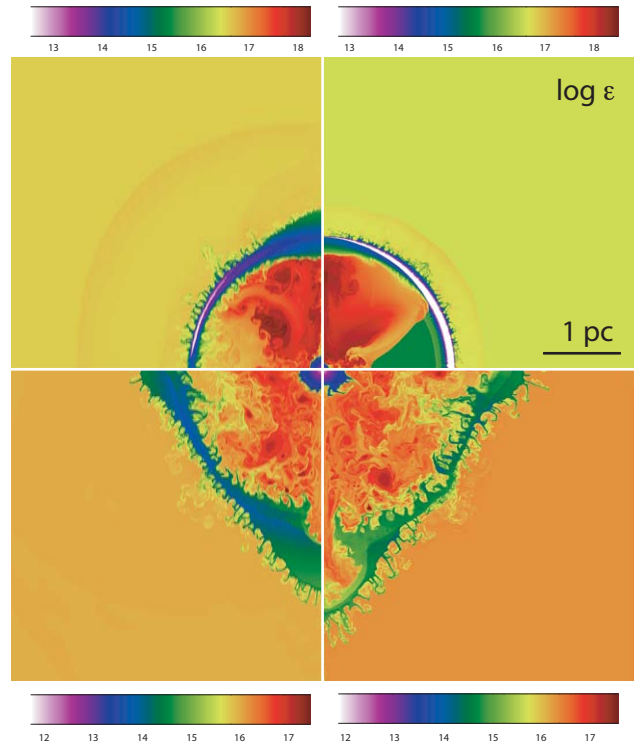


FIG. 8.— The evolution of a GRB remnant inside the wind bubble structure expected around a $35 M_{\odot}$ massive star. The GRB ejecta initial quantities are the same as in Fig. 4. Shown is the evolution of the specific energy, ϵ , in erg/g at $t = 51, 660, 2300$ and 3400 yr. The individual frames have been successively rotated by $\pi/2$. Calculations were done in two-dimensional cylindrical coordinates for eight levels of refinement. The size of the computational domain was $(10 \text{ pc})^2$.

Segura et al. 1996a; García-Segura et al. 1996b). At low metallicity, the RSG phase may be absent; this may also be the case for some binary stars.

As an example, we follow the dynamics of a GRB remnant around a $35 M_{\odot}$ star (as calculated by Chevalier et al. 2004), which evolves (at solar metallicity) through a long-lived RSG stage with prominent consequences for the evolution of the circumstellar matter. The wind velocity in the Wolf-Rayet phase is 10^3 km s^{-1} , and the mass-loss rate $10^5 M_{\odot} \text{ yr}^{-1}$. The ISM pressure and density are assumed to be typical of the hot, low-density phase of a starburst galaxy, with $P_{\text{ISM}} \sim 10^7 \text{ K cm}^{-3}$ and a density of $4 \times 10^{-25} \text{ g cm}^{-3}$. When the fast Wolf-Rayet wind $v_w \sim 10^3 \text{ km s}^{-1}$ starts blowing, it sweeps up the RSG wind material into a shell. The termination shock of the Wolf-Rayet wind is located at $R_t \approx 0.4 \text{ pc}$ and RSG shell at $R_{\text{RSG}} \approx 1.7 \text{ pc}$. Because the pressure in the shocked wind is nearly in equilibrium with the ISM, and the temperature $\sim 10^7 (v_w/10^3 \text{ km s}^{-1})^2 \text{ K}$, the density in the bubble is $\sim 8 \times 10^{25} (P_{\text{ISM}}/10^7) (v_w/10^3 \text{ km s}^{-1})^{-2} \text{ g cm}^{-3}$, independent of the mass-loss rate and the ambient density. The extent of the constant density region is $\sim 4R_t$ out to the dense red supergiant shell.

The resulting evolution a beamed GRB remnant in the circumstellar medium expected around a $35 M_{\odot}$ massive stellar progenitor is summarized in Fig. 8. The presence of the sharp density gradient will only affect the dynamics of the GRB remnant when it size is comparable to, or exceeds, the scale length of the gradient. Before this time, the evolution of the remnant is similar to that depicted in Fig. 4. The

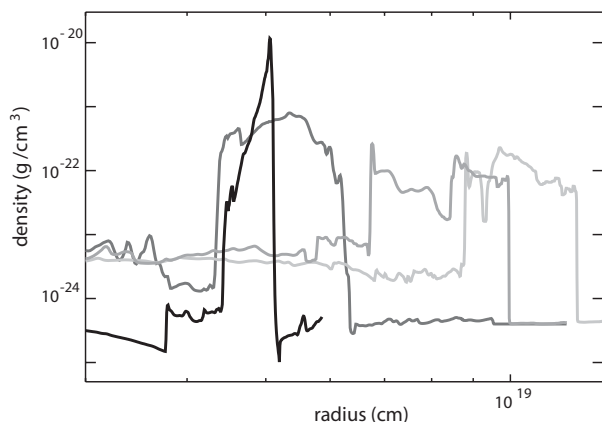


FIG. 9.— The density structure, along the z axis of a GRB remnant interacting with a wind bubble structure. The simulation is the same as in Fig. 8 for $t = 51, 660, 2300$ and 3400 yr.

bow shock propagates in the direction of motion but also perpendicular to it and, over time, wraps around the expanding ejecta. In a wind bubble, the shock front will expand within the stellar wind until it reaches the sharp density discontinuity at about 1.7 pc. The encounter with the RSG shell happens before the GRB remnant has time to expand laterally, which allows for an elongation of the RSG shell in the z axis. A less pronounced elongation is also seen perpendicular to the z axis, which results from the collision on the equator of the two beamed blobs. Superimposed on this large-scale deformation one can also notice the familiar effects caused by the development of Rayleigh-Taylor (R-T) instability. The instability grows rather quickly and within the following 10^3 yr several elongated spikes extend from the shell. At $\approx 2 \times 10^3$ yr, the remnant has a mean radius of 3 pc (Fig. 9) and the spikes are even more pronounced than before. Both shell and R-T spikes advance with a velocity of $300 - 500 \text{ km s}^{-1}$, which is a very small fraction of the random velocities observed in the hot cavity of the remnant. These fast motions are induced by inflection of consecutive shock waves ramming the irregular shell. The pressure in the cavity is almost uniform, whereas the density varies chaotically. The knots of ejecta formed by the R-T instability are believed to be responsible for several forms of observable radiation in some young SNRs, including radio synchrotron and optical emission lines. The sheared motions resulting from the instability could lead to an amplification of the magnetic field strength and enhance the bright radio remnant (Jun & Norman 1996).

The growth time of the instability may be roughly estimated in the following way. The interaction of the GRB remnant with the wind cavity leads to an increase of the shell-driving pressure by

$$\Delta P = \frac{E_j}{2\pi R_{\text{rsg}}^3}. \quad (16)$$

The mass of the shell is equal to

$$M_{\text{rsg}} = \frac{4}{3}\pi R_{\text{rsg}}^3 \rho_{\text{rsg}}. \quad (17)$$

ΔP causes an acceleration g_{rsg} of the shell, satisfying the equation

$$4\pi R_{\text{rsg}}^2 \Delta P = M_{\text{rsg}} g_{\text{rsg}}. \quad (18)$$

With no other forces involved, the contact surface separating

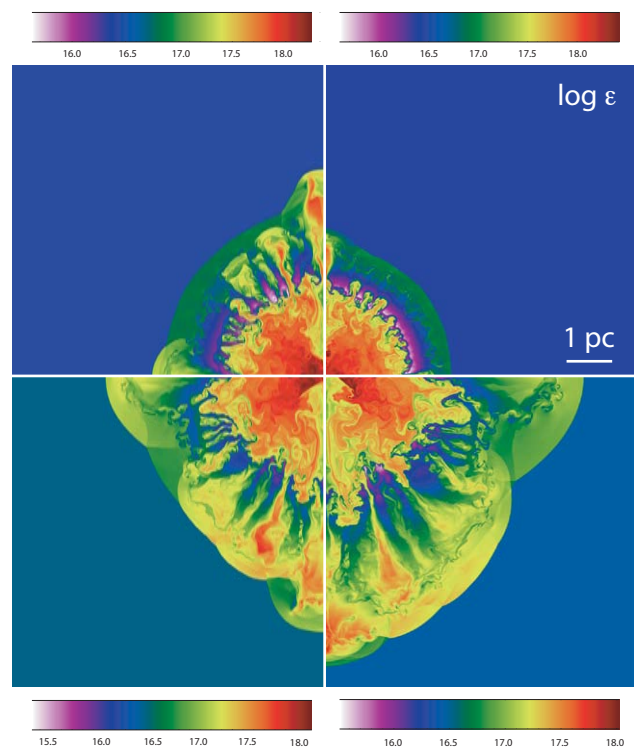


FIG. 10.— The evolution of a GRB remnant accompanied by an underlying spherical supernova. The wind bubble structure as well as the GRB ejecta initial quantities are the same as in Fig. 8. Shown is the evolution of the specific energy, ϵ , in erg/g at $t = 380, 570, 765$ and 950 yr. The individual frames have been successively rotated by $\pi/2$. Calculations were done in two-dimensional cylindrical coordinates for eight levels of refinement. The size of the computational domain was $(20 \text{ pc})^2$.

both fluids is unstable to perturbations of all wavelengths and the fluids interpenetrate. The instability grows exponentially on a characteristic time scale

$$t_{\text{R-T}} = \left(\frac{4\pi^2 \lambda R_{\text{rsg}}^4 \rho_{\text{rsg}}}{3E_j} \right)^{1/2}, \quad (19)$$

where λ is the perturbation wavelength, corresponding to a growth time of

$$t_{\text{R-T}} \approx 10^3 \left(\frac{R_{\text{rsg}}}{2 \text{ pc}} \right)^2 \left(\frac{\lambda}{0.2 \text{ pc}} \right)^{1/2} \rho_{\text{rsg},-21}^{1/2} E_{51}^{1/2} \text{ yr}, \quad (20)$$

where E_{51} is the total energy of the GRB remnant and $\rho_{\text{rsg}} = 10^{-21} \rho_{\text{rsg},-21} \text{ g cm}^{-3}$. Indeed, the observed spikes have dimensions of tenths of parsecs and grow on a time scale comparable to the estimated one. For this discussion we have assumed that the remnant evolution is effectively adiabatic and should be modified to include the effects of radiative cooling⁴, which are expected to become important after about few thousand years.

The disruption of the RSG shell is, as expected, very sensitive to the total amount of energy and momentum released by the GRB explosion. To illustrate this, we study the evolution of a GRB remnant accompanied by an underlying 10^{52} erg SN in a wind bubble structure such as that illustrated in Fig. 8. The large-angle SN outflow, carrying significantly

⁴ For example, the growth of the R-T instability in the radiating shell is found to be higher than in the adiabatic case (Chevalier & Blondin 1995).

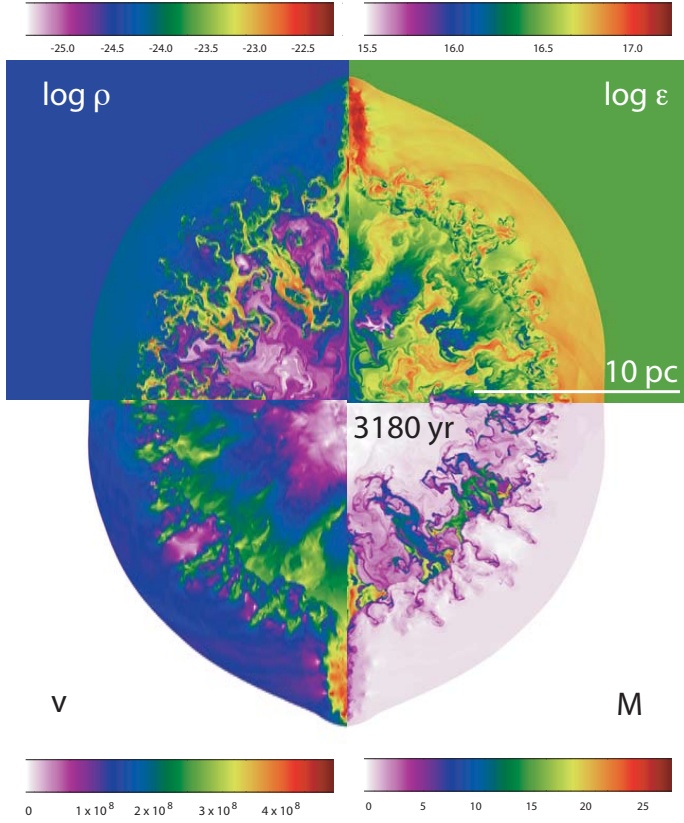


FIG. 11.— The density (ρ), specific energy (ϵ), velocity (v), and Mach number (M) of a GRB remnant accompanied by an underlying spherical supernova ($M_{\text{SN}} \approx 5M_{\odot}$) interacting with a wind bubble structure. The simulation is the same as in Fig. 10 but for $t = 3180$ yr.

more energy and inertia than the relativistic jet itself, sweeps up the GRB ejecta before it is decelerated by the RSG shell. The resultant shell, clearly apparent in the first frame of Fig. 10 taken at $t=380$ yr, will then be pushed outward at faster velocity than it would be in the absence of the SN ejecta. In subsequent evolutionary phases one can observe a broadening of the merged shell, accompanied by a decreased of its density, and the development of small-amplitude density perturbations. After $t = 3180$ yr, the remnant has become highly irregular already when it has grown to ≈ 13 pc, and is also rather weakly elongated in the direction of motion of the beamed ejecta (Fig. 11). There are also multiple kinematic components within the remnant. Fast-moving knots and fast-moving flocculi, dense fragments of SN ejecta, expanding from the explosion center with velocities of several thousand km s^{-1} . Much slower (several hundred km s^{-1}) flocculi are clearly shocked and accelerated remnants of stellar material ejected by the SN progenitor prior to the explosion.

The calculations above demonstrate how the measurable properties of GRB remnants depend on the nature of the progenitor star and the medium around it. Moreover, counts of GRB remnants as a function of age may have huge selection effects, as the actual age of the GRB may be considerably less than the kinematical age estimated from the radius of the filaments divided by the expansion velocity. Although nurture makes a huge difference, hydrodynamical models of young GRB remnants are also sensitive to the structure of the ejecta, which might be rather complicated in detail as demonstrated by inspection of numerical models of SN explosions

TABLE 1
MEAN SPACE DENSITY OF ASYMMETRIC GRB REMNANTS.

	t_{sph}	$\phi_{\text{sph}} [\mathfrak{R}_{\text{grb}} = 1 \text{Gpc}^{-3} \text{yr}^{-1}]$
$k = 0$	$3 \times 10^3 E_{51}^{1/3} \rho_0^{-1/3} \text{ yr}$	$3 \times 10^3 E_{51}^{1/3} \rho_0^{-1/3} f_b^{-1} \mathfrak{R}_{\text{grb}} \text{ Gpc}^{-3}$
$k = 2$	$5 \times 10^4 E_{51} A_*^{-1} \text{ yr}$	$5 \times 10^4 E_{51} A_*^{-1} f_b^{-1} \mathfrak{R}_{\text{grb}} \text{ Gpc}^{-3}$
$R_{\text{rsg}} \sim 1 \text{ pc}$	$10^2 E_{51} A_*^{-1} \text{ yr}$	$10^2 E_{51} A_*^{-1} f_b^{-1} \mathfrak{R}_{\text{grb}} \text{ Gpc}^{-3}$
$E_{\text{sn}} \sim E_{j,51}$	$3 \times 10^3 \text{ yr}$	$3 \times 10^3 f_b^{-1} \mathfrak{R}_{\text{grb}} \text{ Gpc}^{-3}$
$E_{\text{sn}} \geq E_{j,51}$	$\leq 10^3 \text{ yr}$	$\leq 10^3 f_b^{-1} \mathfrak{R}_{\text{grb}} \text{ Gpc}^{-3}$

(e.g. Chevalier & Blondin 1995).

7. GRB REMNANTS AND THEIR DETECTABILITY

7.1. Asymmetric GRB Remnants in the Local Universe

It is obvious from the discussions in this paper that the dynamics of GRB remnants are complex, especially because of rich interactions between the ejecta and the circumburst medium. The structure of ejecta is also important, in particular for young GRB remnants. Abundant confirmation was provided of the important notion that the morphology and visibility of GRB remnants are determined largely by their circumburst environment, from the initial density gradient created by the progenitor to the effects of large- and small-scale circumburst structures in later evolution. This distribution is expected to be nonuniform around massive GRB progenitors because of the significant mass loss and the dynamical effects of the stellar winds.

The presence of a density gradient will only affect the dynamics of a GRB when the remnant size is comparable to, or exceeds, the scale length of the gradient. Before this time, the density can be treated as approximately uniform. In the absence of characteristic scales in stellar ejecta and in the ambient medium, self-similar, spherically symmetric solutions exist, and they are widely used to interpret observational data on young GRB remnants. However, even for the simplest density distributions, we found that the resulting structure and dynamics of their remnants are very different from the standard self-similar solutions. This is mainly because at early stages the morphology of a beamed GRB remnant would be very different from that of a spherical explosion. In principle, this can be used to identify those remnants although the dynamical complexity of their surrounding circumburst medium seriously limits our ability to decipher their presence, in particular around massive star progenitors.

The values of the mean space density, ϕ_{sph} , of asymmetric GRB remnants expanding into a variety of circumburst environments are given in Table 1. Taking the long GRB rate expected in the local universe to be $\mathfrak{R}_{\text{grb}} = 0.3 \text{ Gpc}^{-3} \text{ yr}^{-1}$ (Guetta & Piran 2007), an upper limit to the number density of asymmetric remnants arising from massive stellar progenitors is

$$\phi_{\text{sph}} \approx 5 \times 10^{-3} E_{51} A_*^{-1} \frac{f_b^{-1}}{100} \text{ Mpc}^{-3}. \quad (21)$$

This is a generous upper limit, since it assumes that all long GRBs occur in a free $1/r^2$ stellar wind and that the relativistic component is energetically dominant. For comparison, an ultraconservative lower limit to the space density of long GRBs gives

$$\phi_{\text{sph}} \approx 10^{-5} \frac{f_b^{-1}}{100} \text{ Mpc}^{-3}. \quad (22)$$

With the rates given by Guetta & Piran (2005), the frequency

of short GRBs is about 20 times higher than that of long GRBs. The much lower external density (likely uniform) medium expected around short GRBs (e.g., Lee et al. 2005) suggests

$$\phi_{\text{sph}} \approx 6 \times 10^{-3} E_{51}^{1/3} \rho_{-3}^{-1/3} \frac{f_b^{-1}}{10} \text{Mpc}^{-3}, \quad (23)$$

where $\rho_{-3} = 10^{-3} \rho_0$. Thus the rate of asymmetric short GRB remnants could be much higher than equation (22). However, the remnant's visibility would be highly biased in favor of those with massive progenitors.

7.2. Observational Prospects

The most difficult task at present is to relate hydrodynamical modeling to observations. A few of the observables, such as expansion rates and thicknesses of the flow structures, can be relatively easily determined from the models. However, modeling radio and X-ray emission is in general difficult, as we are still lacking an understanding of how electrons are accelerated in shocks. Very similar difficulties are encountered in modeling nonthermal X-rays. Thermal X-ray spectra are in principle easier to model, but in practice the difficulties are formidable. The reason for these difficulties is our poor understanding of a number of topics, such as the amount of electron heating in collisionless shocks, the detailed structure and composition of ejecta, their clumping, the presence of the inhomogeneous circumstellar medium, and the presence of dust.

The difficult task of interpreting observations with the help of hydrodynamical models is perhaps best illustrated by Cas A. This is a remnant of a massive star explosion and a classic prototype shell supernova remnant. It has been detected throughout the whole electromagnetic spectrum (Ryle & Smith 1948; Ashworth 1980; Aharonian et al. 2001; Fesen 2001; Hwang et al. 2004). Observations in various wavelength bands probe very different components of the remnant: synchrotron radio emission gives us information about relativistic electrons, thermal X-ray emission is produced by the bulk of the shocked hot gas, much cooler gas in radiative shocks emits at optical wavelengths, and observations in infrared reveal still cooler gas and dust. However, we still do not understand what is the relationships between all these features and the remnant's hydrodynamics (e.g. Hwang et al. 2004).

To estimate the emissivity of GRB remnant without undertaking the complicated effort of calculating X-ray spectra, we have summed up the internal energy density of the gas, ϵ_{int} , for each zone in the simulations and plotted $L_X \sim f_X \epsilon_{\text{int}}$ as a function of time in Fig. 12, where $f_X \sim 0.01$ is the fraction of internal energy that is radiated away in the 0.3-10 keV range. This is only a very approximate procedure and should be taken as an order of magnitude estimate at present. Superimposed on these plots, on a common scale, are all GRB afterglows with X-ray luminosity measurements covering several tens of days. There are, unfortunately, only a few curves, because such measurements can only be made on GRBs that are relatively nearby, but their light curves should be illustrative. We then compared these X-ray lightcurves with those of supernovae and historical Galactic SN remnants. The resulting plot is striking in several ways. Despite the huge disparity in initial appearance, there are indications of a common convergence of all classes of phenomena to a common resting place: $L_X \sim 10^{39} - 10^{40} \text{ erg s}^{-1}$ about a few years after the explosive

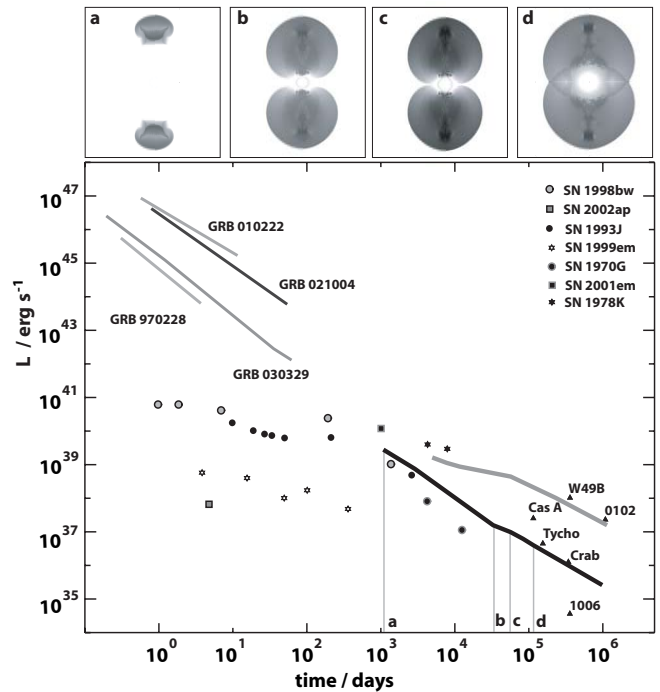


FIG. 12.— Compilation of GRB, supernova and SN remnant X-ray light curves (0.3- 10 keV) presented as (isotropic) luminosity distances as a function of age (adapted from Kouveliotou et al. 2004; Immler & Kuntz 2005). Superimposed on these plots, on a common scale, is the schematic lightcurves of two GRB remnants expanding into different external density environments. The inset figures show the evolution of the GRB remnant in a $1/r^2$ density profile (the simulation is the same as in Fig. 4). The grey curve shows the evolution of a GRB remnant in a pre-existing wind-bubble (the simulation is the same as in Fig. 8). To estimate the X-ray lightcurves, we have summed up the internal energy density of the gas, ϵ_{int} , for each zone in the simulations and plotted $L_X \sim f_X \epsilon_{\text{int}}$ as a function of time, where $f_X \sim 0.01$ is the fraction of internal energy that is radiated away in the 0.3-10 keV range.

event. Moreover, it clearly illustrates that the transition from a GRB to a SN remnant appears to be rather smooth. Clearly, detailed studies relating hydrodynamical modeling to observations are needed to study the transition from a GRB into a stellar remnant.

Fig. 12 shows the schematic lightcurves of two GRB remnants expanding into different external density environments. For a $1/r^2$ density profile, as in the black curve of Fig. 12, the luminosity of the remnant is initially dominated by the emission of the individual beamed components as they interact with the stellar wind. The luminosity continues with a quasi-steady decay rate until the individual beamed components collide to form a single structure. The resultant lightcurve will then be characterized by a modest increase in luminosity. For a GRB expanding inside a pre-existing wind-bubble, as in the grey curve of Fig. 12, the resultant lightcurves can evolve much faster into luminous remnants such as Cas A (Hwang et al. 2004) or W49B (Miceli et al. 2006) due to their strong interaction with the dense circumburst medium.

This plot summarized many of the issues outlined in this paper, in which we argued that the morphology and visibility of GRB remnants are governed by the pre-existing structure of their birthplace environments. Since GRB remnants result from the impact of their ejecta with circumstellar gas, their visibility is highly biased in favor of those with massive progenitors. Many young GRBs from massive progenitors would be bright because their ejected mass is interacting with nearby

gas expelled by the progenitor itself. This circumstellar gas is likely to have mass comparable to that of the accompanied SN debris and will not extend much further than a few parsecs. After less than a century, the blast wave from the GRB will pass through this relatively dense circumstellar gas. Inferring the presence of a beamed component in these hypernova scenarios would be challenging. The number density of asymmetric GRB remnants in the local Universe could be far larger if they expand in a tenuous interstellar medium as expected, for example, in the merger of two neutron stars (although there are reasons to suspect that the ejecta may not be too narrowly beamed) and may be easier to constrain directly (acknowledging the obvious trade-offs in sensitivity and angular

resolution, particularly for radio and X-ray observations).

We have benefited from many useful discussions with C. Fryer, J. Granot, T. Piran and S. Woosley. We are especially grateful to W. Zhang for countless insightful conversations. The software used in this work was in part developed by the DOE-supported ASCI/Alliance Center for Astrophysical Thermonuclear Flashes at the University of Chicago. Computations were performed on the IAS Scheide computer cluster. This work is supported by NSF: PHY-0503584 (ER-R) and DOE SciDAC: DE-FC02-01ER41176 (ER-R and AM).

REFERENCES

- Aharonian, F., et al. 2001, *A&A*, 370, 112
 Ashworth, W. B., Jr. 1980, *Journal for the History of Astronomy*, 11, 1
 Ayal, S., & Piran, T. 2001, *ApJ*, 555, 23 (AP01)
 Begelman, M. C., Blandford, R. D., & Rees, M. J. 1984, *Rev. Mod. Phys.*, 56, 255
 Belczynski, K., Perna, R., Bulik, T., Kalogera, V., Ivanova, N., & Lamb, D. Q. 2006, *ApJ*, 648, 1110
 Bjorkman, J. E., & Cassinelli, J. P. 1993, *ApJ*, 409, 429
 Blandford, R. D., & McKee, C. F. 1976, *Phys. Fluids*, 19, 1130
 Bloom, J. S., Sigurdsson, S., & Pols, O. R. 1999, *MNRAS*, 305, 763
 Cannizzo, J. K., Gehrels, N., & Vishniac, E. T. 2004, *ApJ*, 601, 380
 Chevalier, R., & Blondin, J. M. 1995, *ApJ*, 444, 312
 Chevalier, R. A., & Li, Z. 2000, *ApJ*, 536, 195
 Chevalier, R. A., Li, Z., & Fransson, C. 2004, *ApJ*, 606, 369
 Chiosi, C., & Maeder, A. 1986, *ARA&A*, 24, 329
 Fabian, A. C., Stewart, G. C., & Brinkmann, W. 1983, *Supernova Remnants and their X-ray Emission*, 101, 119
 Fesen, R. A. 2001, *ApJS*, 133, 161
 Fryer, C. L., Woosley, S. E., & Hartmann, D. H. 1999, *ApJ*, 526, 152
 García-Segura, G., Langer, N., & Mac Low, M. M. 1996a, *A&A*, 316, 133
 García-Segura, G., Mac Low, M. M., & Langer, N. 1996b, *A&A*, 305, 229
 Gorosabel, J., et al. 2006, *ApJ*, 641, L13
 Granot, J., Miller, M., Piran, T., Suen, W. M., & Hughes, P. A. 2001, *Gamma-ray Bursts in the Afterglow Era*, 312
 Granot, J., & Loeb, E. 2001, *ApJ*, 551, L63
 Granot, J., & Ramirez-Ruiz, E. 2004, *ApJ*, 609, L9
 Granot, J., Ramirez-Ruiz, E., & Loeb, A. 2005, *ApJ*, 618, 413
 Granot, J. 2007, *Revista Mexicana de Astronomia y Astrofisica*, 27, 140
 Guetta, D., & Piran, T. 2005, *A&A*, 435, 421
 Guetta, D., & Piran, T. 2007, *Journal of Cosmology and Astro-Particle Physics*, 7, 3
 Hjorth, J., et al., 2004, *Nature*, 423, 847
 Hwang, U., et al. 2004, *ApJ*, 615, L117
 Immler, S., & Kuntz, K. D. 2005, *ApJ*, 632, L99
 Jun, B.-I., & Norman, M. L. 1996, *ApJ*, 472, 245
 Kaneko, Y., et al. 2007, *ApJ*, 654, 385
 Kouveliotou, C., et al. 2004, *ApJ*, 608, 872
 Langer, N. 1998, *A&A* 329, 551
 Lee, W. H., Ramirez-Ruiz, E., & Granot, J. 2005, *ApJ*, 630, L165
 Lee, W. H., & Ramirez-Ruiz, E. 2007, *New Journal of Physics*, 9, 17
 MacFadyen, A. I., & Woosley, S. E., 1999, *ApJ*, 524, 262
 MacFadyen, A. I., Woosley, S. E., & Heger, A. 2001, *ApJ*, 550, 410
 Mazzali, P. A., et al. 2006, *ApJ*, 645, 1323
 Miceli, M., et al. 2006, *A&A*, 453, 567
 Mirabel, I. F., & Rodríguez, L. F. 1999, *ARA&A*, 37, 409
 Oren, Y., Nakar, E., & Piran, T. 2004, *MNRAS*, 353, L35
 Pian, E., et al. 2006, *Nature*, 442, 1011
 Ramirez-Ruiz, E., Dray, L., Madau, P., & Tout, C. A. 2001, *MNRAS*, 327, 829
 Ramirez-Ruiz, E., Celotti, A., & Rees, M. J. 2002, *MNRAS*, 337, 1349
 Ramirez-Ruiz, E., García-Segura, G., Salmonson, J. D., & Pérez-Rendón, B. 2005, *ApJ*, 631, 435
 Rhoads, J. E. 1999, *ApJ*, 525, 737
 Ryle, M., & Smith, F. G. 1948, *Nature*, 162, 462
 Sari, R., Piran, T., & Halpern, J. P. 1999, *ApJ*, 519, L17
 Soderberg, A. M., et al. 2004, *Nature*, 430, 648
 Stanek, K. Z., et al., 2003, *ApJ*, 591, L17
 van Marle, A. J., Langer, N., Achterberg, A., & García-Segura, G. 2006, *A&A*, 460, 105
 Waxman, E. 1997, *ApJ*, 491, L19
 Waxman, E., Frail, D., & Kulkarni, S. 1998, *ApJ*, 497, 288
 Wijers, R. A. M. J. 2001, in *Gamma Ray Bursts in the Afterglow Era*, ed. E. Costa, Frontera F. and Hjorth J. (Springer: Berlin), 306
 Woosley, S. E. 1993, *ApJ*, 405, 273
 Woosley, S. E., & Bloom, J. S. 2006, *ARA&A*, 44, 507